Supporting Information

In situ construction of a MOF-derived carbon-encapsulated $LiCoO_2$ heterostructure as a superior cathode for elevated-voltage lithium storage: from experimental to theoretical study

Jia Lin,[ab] Chenghui Zeng,[b] Yueying Chen,[a] Xiaoming Lin,*[a] Chao Xu*[a] and Cheng-Yong Su*[c]

[a] Guangzhou Key Laboratory of Materials for Energy Conversion and Storage, Key Laboratory of Theoretical Chemistry of Environment, Ministry of Education, School of Chemistry, South China Normal University, Guangzhou 510006, China

[b] College of Chemistry and Chemical Engineering, Key Laboratory of Functional Small Organic Molecule, Ministry of Education and Jiangxi's Key Laboratory of Green Chemistry, Jiangxi Normal University, Nanchang 330022, China

[c] MOE Laboratory of Bioinorganic and Synthetic Chemistry, Lehn Institute of Functional Materials, School of Chemistry, Sun Yat-Sen University, Guangzhou 510275, China

AUTHOR INFORMATION

E-mail: linxm@scnu.edu.cn; chaoxu@m.scnu.edu.cn; cesscy@mail.sysu.edu.cn

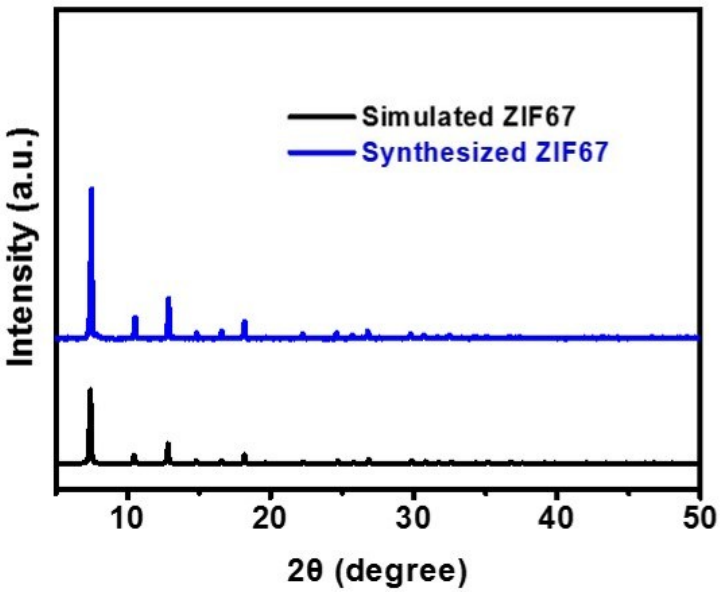

Fig. S1 XRD patterns of as-synthesized and simulated ZIF67.

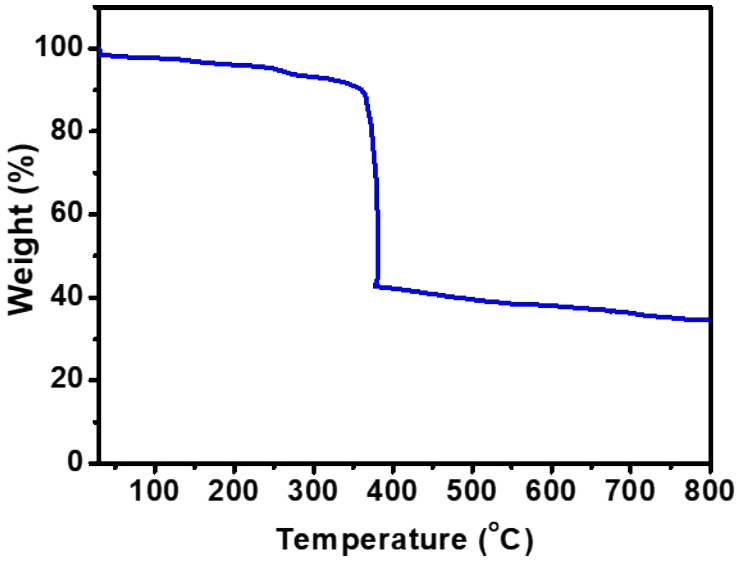

Fig. S2 TGA plot of the ZIF67 under air atmosphere.

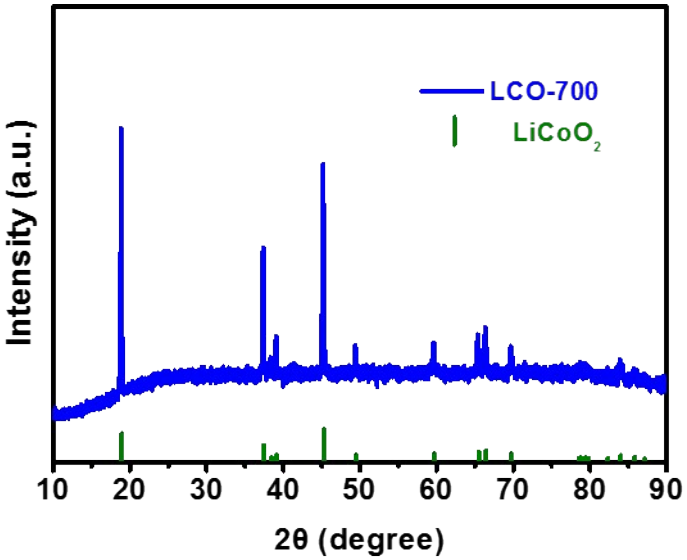

Fig. S3 XRD pattern of MOF-derived LCO-700 sample.

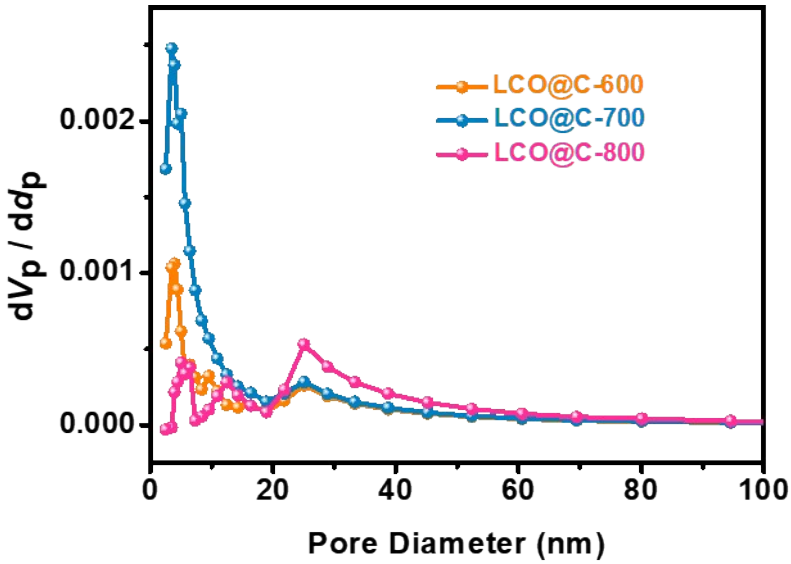

Fig. S4 Pore-size distribution curves of the LCO@C-600, -700, and -800, respectively.

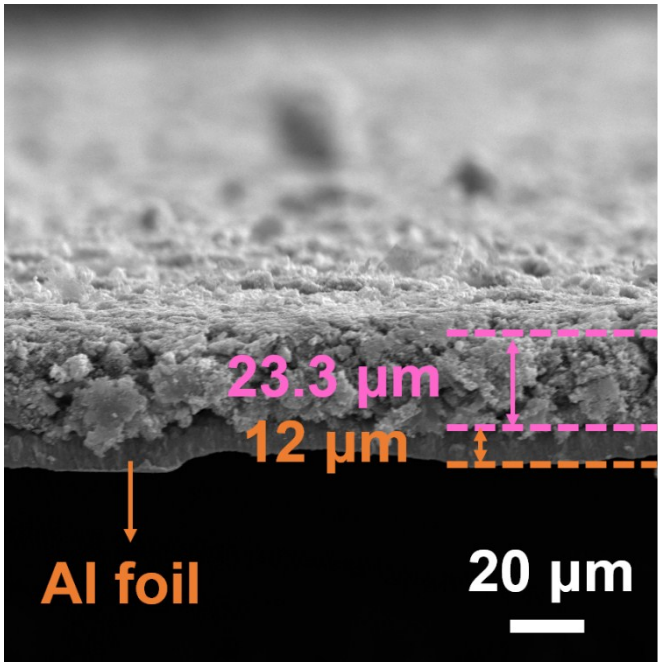

Fig. S5 The cross-section view SEM image of the LCO@C-700 electrode film.

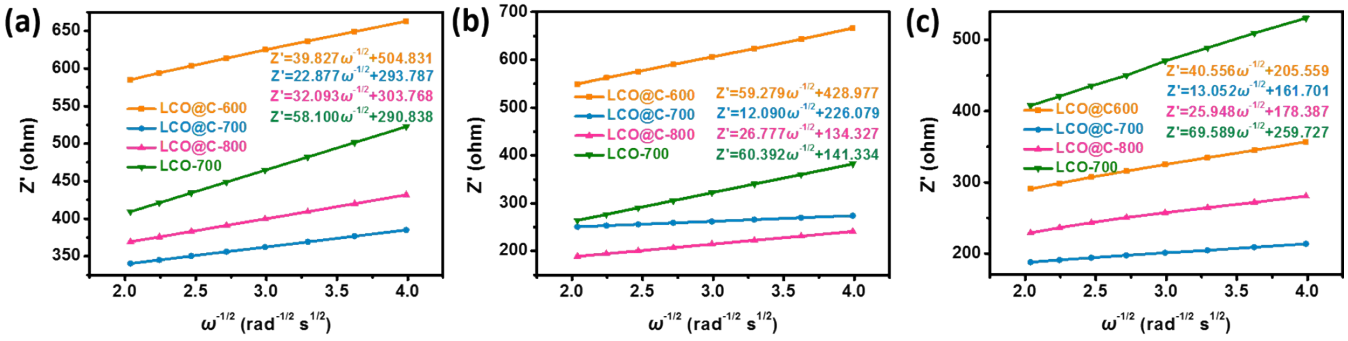

Fig. S6 The relationship of Z' and $\omega^{-1/2}$ of LCO@C-600, -700, -800, and LCO-700 after (a) 1st cycle, (b) 100th cycle, and (c) 200th cycle.

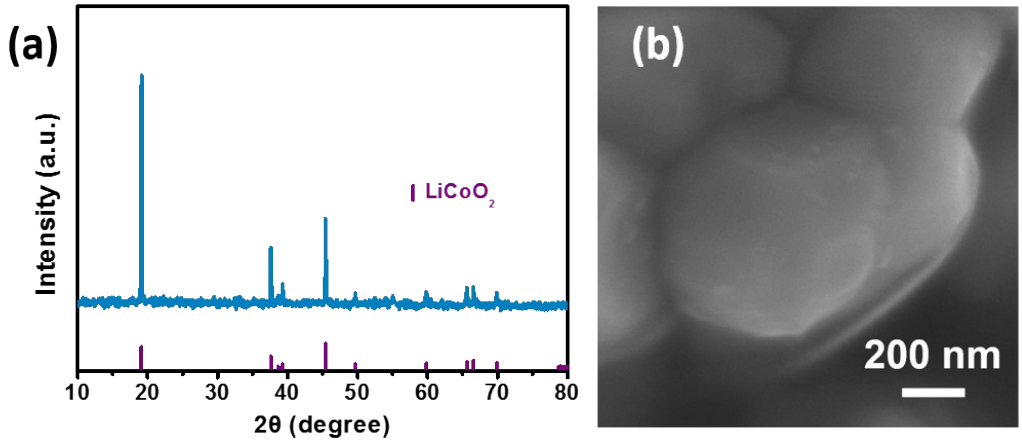

Fig. S7 (a) XRD pattern and (b) SEM image of the LCO@C-700 electrode material scraped down of the electrode films after 200 cycles, respectively.

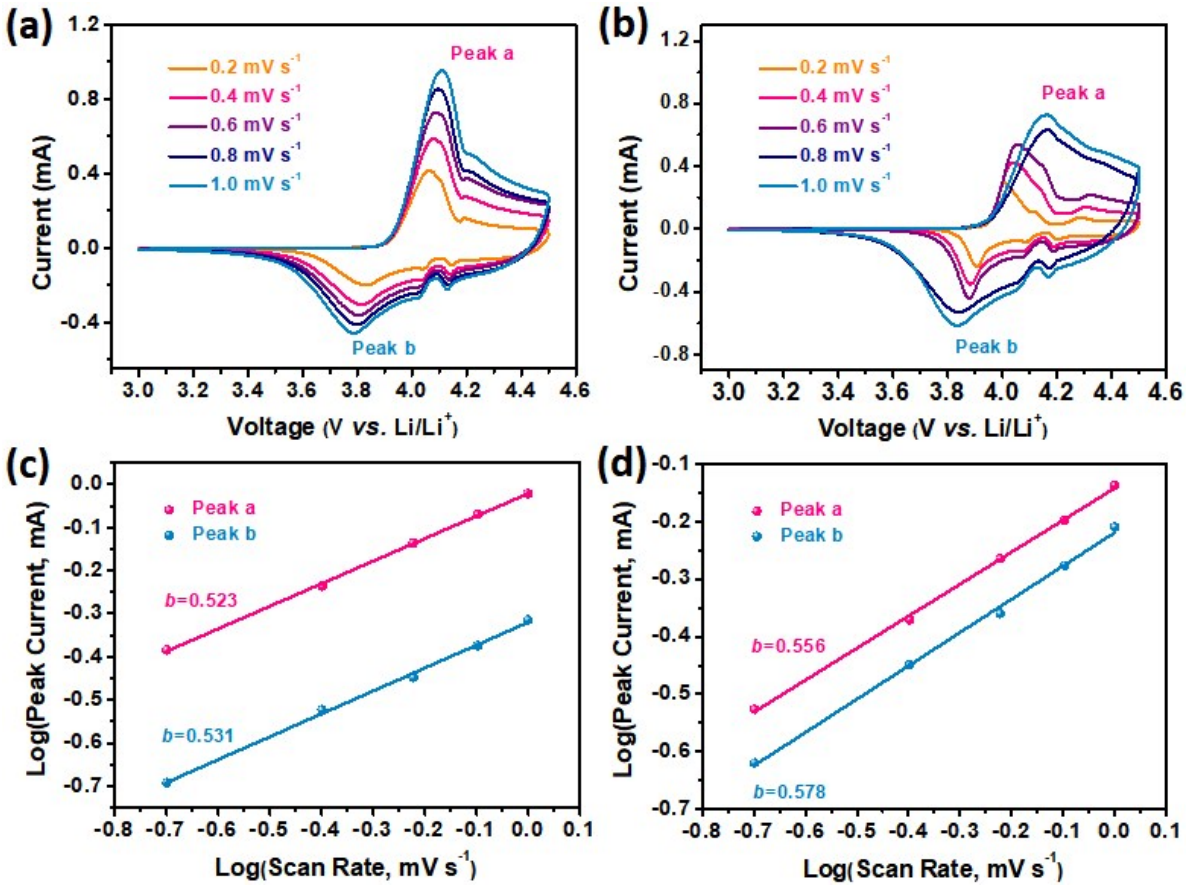

Fig. S8 CV curves and the liner relationships of the main cathodic and anodic peaks at the different scan rates from 0.2 to 1.0 mV s^{-1} for (a and c) LCO-700 and (b and d) LCO@C-600, respectively.

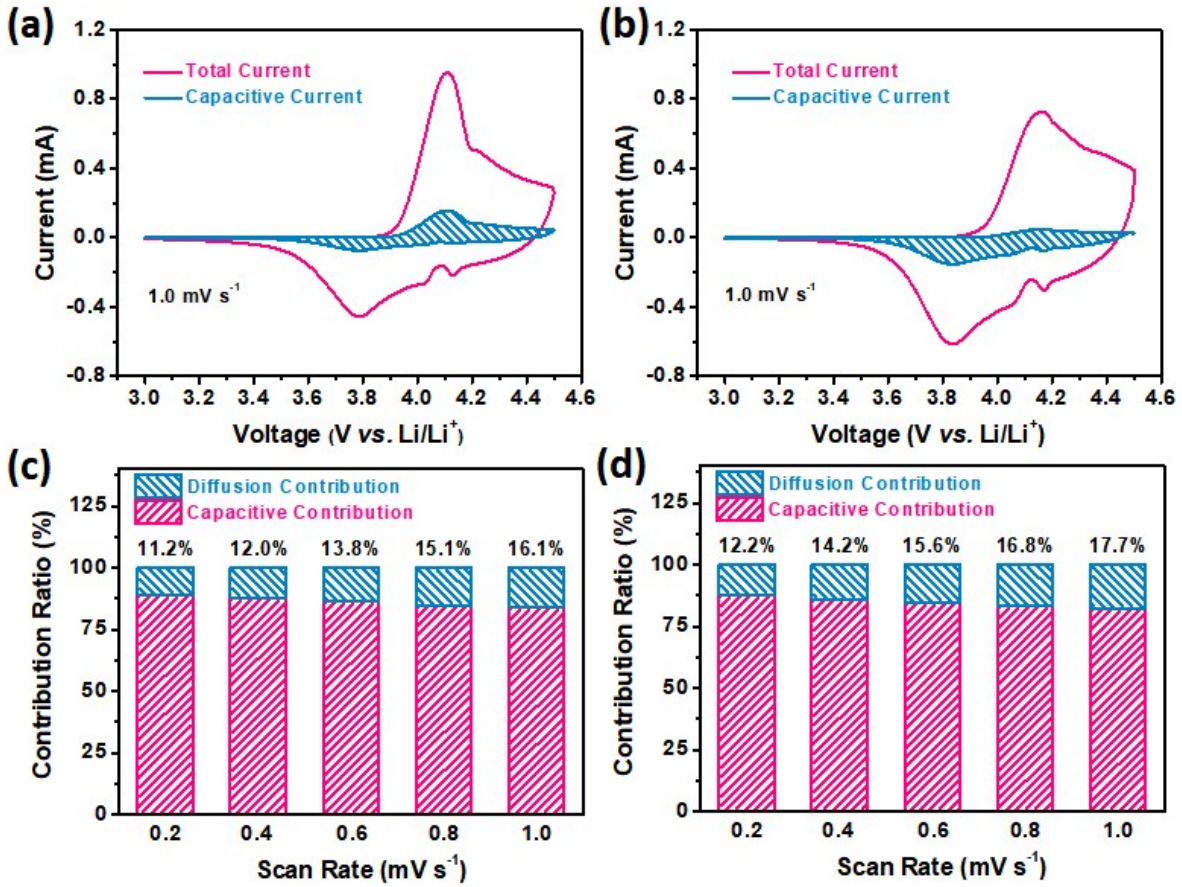

Fig. S9 The CV curve separation of the pseudocapacitive current and total current contribution at 1.0 mV s^{-1}, and contribution ratio of the diffusion- and pseudocapacitive-controlled capacities at different scan rates for (a and c) LCO-700 and (b and d) LCO@C-600, respectively.

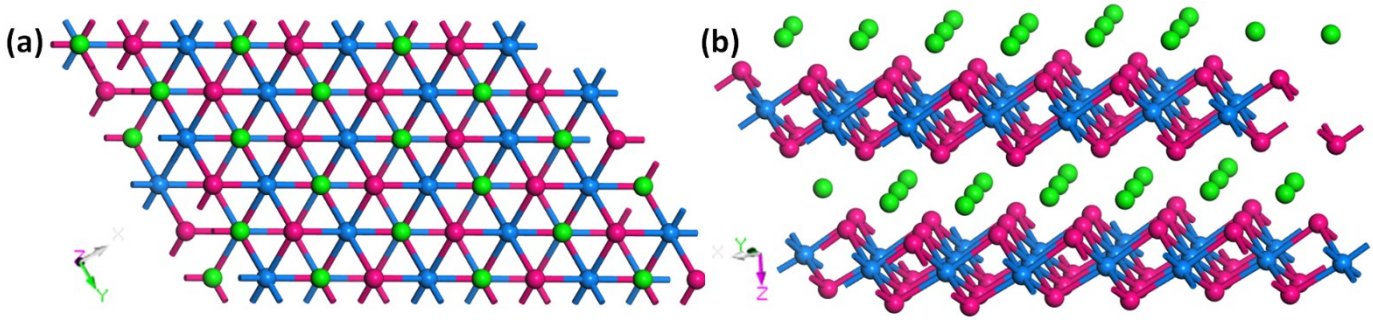

Fig. S10 Cluster structure of sole $LiCoO_2$ from the (a) top and (b) side view. The big green, pink, and blue spheres represent for Li, O, and Co atoms, respectively.

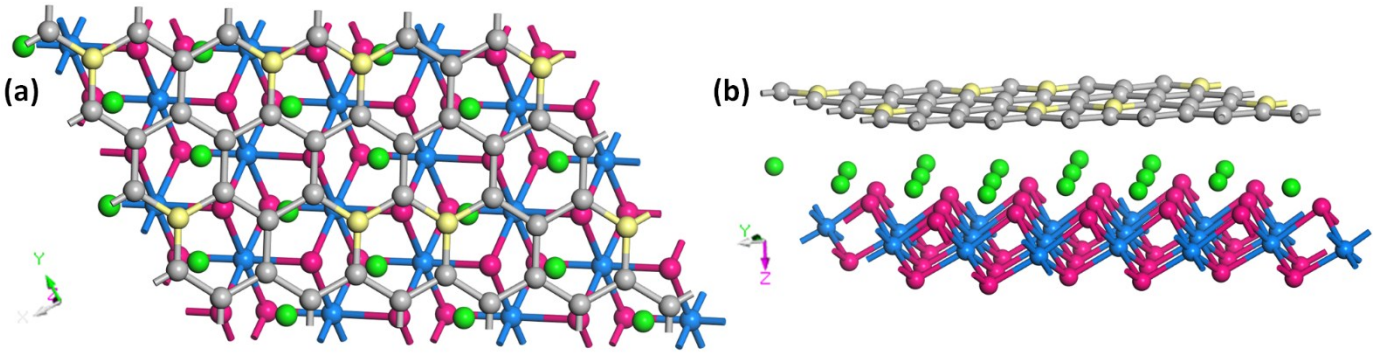

Fig. S11 Cluster structure model of the LCO@C heterostructure from the (a) top and (b) side view. The big green, grey, yellow, pink, and blue spheres represent for Li, C, N, O, Co and atoms, respectively.

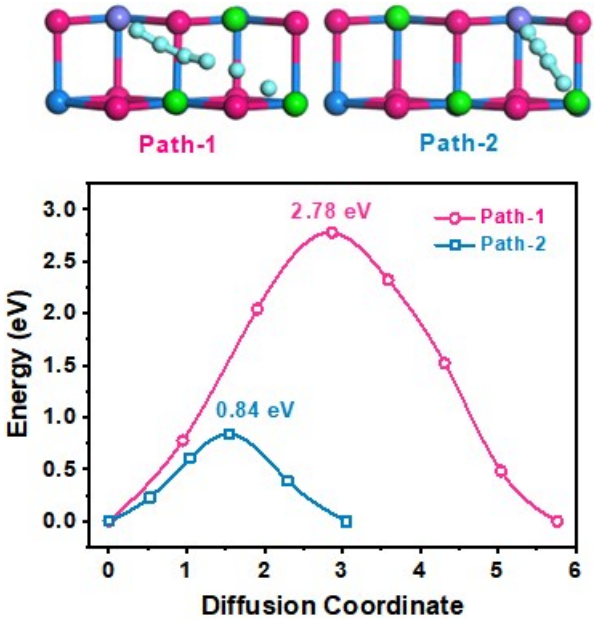

Fig. S12 The Li-vacancy migration paths and corresponding calculated diffusion energy barrier profiles of sole $LiCoO_2$ from DFT calculations.

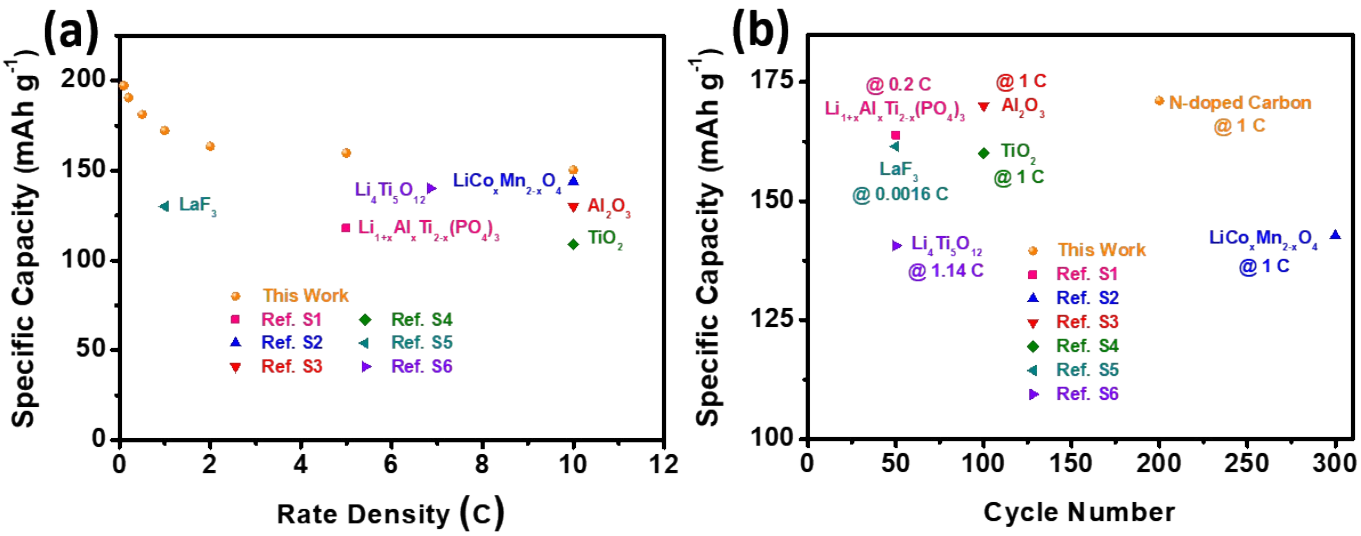

Fig. S13 Comparison of the rate capability and long-cycling performance of the surface-coating LCO at an elevated cut-off voltage of 4.5 V.

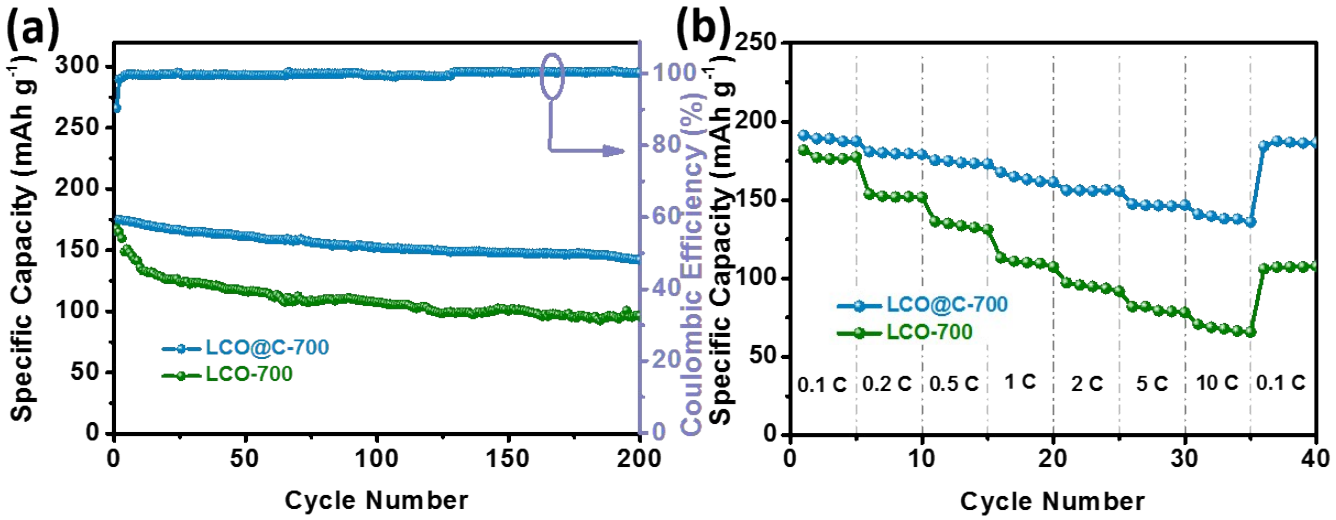

Fig. S14 (a) Cyclability at the current density of 2 C, (b) rate capability at different current rates ranging from 0.1 C to 10 C of the LCO@C-700 and LCO-700 cathode films which includes 92 wt% active material, 4 wt% PVDF, and 4 wt% Super P.

Table S1 Crystallographic data obtained from detailed Rietveld refinement result of the LCO@C-600, -700, and -800 samples.

	a-axis (Å)	***c***-axis (Å)	V (Å^3)	R_{wp} (%)	R_p (%)
LCO@C-600	2.8300	14.12519	97.73	4.47	3.38
LCO@C-700	2.8167	14.08632	96.85	2.35	1.36
LCO@C-800	2.8205	14.10774	97.08	3.25	2.21

Table S2 The fitted results of impedance spectra by the equivalent circuit as inset in Fig. 4g.

	Impedance (Ω)											
	LCO@C-600			LCO@C-700			LCO@C-800			LCO-700		
	R_e	R_{sf}	R_{ct}	R_e	R_{sf}	R_{ct}	R_e	R_{sf}	R_{ct}	R_e	R_{sf}	R_{ct}
1st cycle	2.9	151.9	384.8	2.59	111.7	163.3	2.8	107.9	241.4	8.3	146.9	166.2
100th cycle	5.1	146.2	228.2	2.8	87.2	106.1	3.3	174.9	127.2	9.0	109.1	393.6
200th cycle	2.3	102.8	852.1	2.4	63.4	65.2	4.0	118.7	92.2	7.7	158.2	768.9

Table S3 Lithium ion diffusion coefficients at various stages after discharged cycling calculated by the EIS results.

	Lithium Ion Diffusion Coefficient (D_{Li}, cm^2 s^{-1})			
	LCO@C-600	LCO@C-700	LCO@C-800	LCO-700
1st cycle	$6.54*10^{-9}$	$1.98*10^{-8}$	$1.01*10^{-8}$	$3.07*10^{-9}$
100th cycle	$2.95*10^{-9}$	$7.10*10^{-8}$	$1.45*10^{-8}$	$2.84*10^{-9}$
200th cycle	$6.31*10^{-9}$	$6.09*10^{-8}$	$1.54*10^{-8}$	$2.14*10^{-9}$

References:

S1 Q. Yang, J. Huang, Y. Li, Y. Wang, J. Qiu, J. Zhang, H. Yu, X. Yu, H. Li and L. Chen, *J. Power Sources*, 2018, **388**, 65–70.

S2 R. Gu, Z. Ma, T. Cheng, Y. Lyu, A. Nie and B. Guo, *ACS Appl. Mater. Interfaces*, 2018, **10**, 31271–31279.

S3 A. Zhou, Q. Liu, Y. Wang, W. Wang, X. Yao, W. Hu, L. Zhang, X. Yu, J. Li and H. Li, *J. Mater. Chem. A*, 2017, **5**, 24361–24370.

S4 A. Zhou, Y. Lu, Q. Wang, J. Xu, W. Wang, X. Dai and J. Li, *J. Power Sources*, 2017, **346**, 24–30.

S5 Z. Yang, Q. Qiao and W. Yang, *Electrochim. Acta*, 2011, **56**, 4791–4796.

S6 J.-H. Shim, J. Lee, S. Y. Han and S. Lee, *Electrochim. Acta*, 2015, **186**, 201–208.